# Shear Lag Analysis by Adaptive Finite Element Method Part 2: Analysis of Complex Plated Structures

C. K. Lee[1] and G. J. Wu

School of Civil and Structural Engineering
Nanyang Technological University
Nanyang Avenue
Singapore 639798

[1]Email address: ccklee@ntu.edu.sg

Pre-printed version for the paper appeared in the journal
Thin-Walled Structures, Vol. 38, 2000, 311-336

**Summary**

The adaptive finite element analysis procedure proposed in Part 1 of this study is employed to solve the shear lag problems for complex plated structures with more general and complex geometries including core walls with openings, multi-cell box girders and box girders with curved flanges. By using the adaptive finite element method, parametric studies were carried out to investigate the influence of some key geometrical parameters on the shear lag effect for these types of structures. In addition, it is found that the adaptive finite element method is a convenient tool for the shear lag analysis of structures with complicated geometry and multiple loading conditions and could be used in day-to-day analyses.

***Keywords: Adaptive finite element analysis procedure, shear lag analysis, core wall with openings, multi-cell box and curved horizontal girder***

## 1. Introduction

The shear lag phenomenon, which commonly occurs in thin-walled structures, is not only restricted in plated structures with simple geometry. It will also cause stability and serviceability problems for complex plated structures with complicated geometry. Due to the complicated geometry and the coupling of bending and torsional stresses, it is almost always too difficult to apply classical analytical methods [1-5] for the solution of shear lag problems for this type of structures. In this paper, the adaptive finite element analysis procedure used in Part 1 of this study [6], which has been successfully employed to solve the shear lag problem of simple plated structures, will be extended to the case of complex plated structures. For complex plated structures with complicated geometry, the shear lag problem in general cannot be simplified to the 2D plane stress model. Instead, the more complicated 3D thick shell model [7] has to be employed and the six-node thick shell element [8-10] will be used during the adaptive refinement analysis. When comparing with the simple case, since the more complicated thick shell elements are used, the shear lag analysis of complex plate structures will inevitably require more computational cost. However, all advantages of the adaptive refinement procedure identified during the study of simple cases [6], including minimum amount of input data for the initial mesh, the assurance of results with predetermined accuracy and fast analysis for multiple loading case and parametric studies, are all retrained for the case of complex structures. In this paper, concentration will be focused on the solution of the following complex plated structures which are commonly encountered in practical engineering problems. They are, namely,

(1) core wall with openings,

(2) multi-cell box girders, and

(3) horizontal curved box girders.

Parametric studies will be carried out to identify the key geometrical parameters that will affect the shear lag effects of these types of structures. In all the numerical studies carried out, in order to ensure that accurate solutions are obtained, the allowable discontinuous error [6], $e_a$, will be set equal to 5%.

## 2 Shear lag in core walls

In this section, a number of parametric studies will be carried out to study the shear lag effect in core walls with openings (Fig.1 ). Fig. 2 shows the adaptive refinement meshes used in the studies of a core wall with openings. Due to symmetry, only half of the core wall will be modelled model. For core wall structures, the shear lag effect can again be evaluated by the classical concept of effective breadth ratio $\psi$ [6]. In order to allow for a more detailed study of the shear lag effect, a dimensionless shear lag coefficient $\alpha$ [5] will also be employed to measure shear lag in the flange panels. $\alpha$ is defined as the largest fractional reduction in the longitudinal stress comparing with the maximum stress at the web-flange junction (Fig. 3). From Fig. 3, which shows the typical distribution of longitudinal stress across the flange panel, it can be seen that the greater the shear lag effect, the greater the stress reduction. Thus, the largest reduction in stress may be taken as a measure of the degree of shear lag and $\alpha=0$ implies that no shear lag occurs.

In general, the degree of shear lag varies along the height of core walls and will depend on a few parameters:

(1) The web width/flange width ratio (b/a).

(2) The height/flange width ratio (H/a).

(3) The opening size, s.

(4) The loading case.

In this section, triangularly distributed loading is considered as the main loading type which corresponding to the practical wind forces. The loads are applied laterally to the web panels in their in-plane directions, as shown in Fig. 1. The bases of the models are assumed to be perfectly fixed.

## 2.1 Effects of the ratios b/a and H/a on $\alpha$

Firstly, the parameters studied are the web width/flange width ratio (b/a) and the height/flange width ratio (H/a). Totally 35 models were analyzed. The web width/flange width ratios of the models were changed from 1/3 to 3, while the height/flange width ratios were changed from 2 to 14. The flange and web panels were assumed to have the same constant thickness along the height of the wall, and Poisson ratio was taken to be 0.3 throughout. All the openings have the same sizes of s=0.4a and a=4 meters (Fig. 4). The shear lag coefficient $\alpha$ was calculated and plotted against H/a in Fig. 5. It can be seen that $\alpha$ depends mainly on the ratio H/a. The ratio b/a only slightly affect the value of $\alpha$. Fig. 5 also shows that $\alpha$ generally increases from the fixed end to the free end. It should be noted that the longitudinal stress across the flange gradually decreases as the distance from the fixed end increases. The stresses at the center or at the junction continue to drop to zero and even change sign near the free end. In this situation, the value of $\alpha$ will exceed 1 (Fig. 5c). Furthermore, it is found that positive shear lag occurs in near the fixed end, while negative shear lag [11-13] will take place at where both the stresses at the center and at the junction change sign. The distances from the fixed end to the cross-section where negative shear lag occur are different for the different values of H/a and b/a.

## 2.2 Effects of the sizes of the openings

In this section, shear lag analyses were carried out for a core wall with b/a=1 and H/a=10. The sizes of the openings were changed from 0 to 0.5a. The shear lag coefficients obtained are shown in Fig. 6. It can be seen that the opening sizes have large influence on $\alpha$. The larger the opening size, the severer the shear lag effect. Particularly, when the opening size is larger than 0.5a, nearly all the longitudinal stresses at the center of the flange change sign from positive to negative such that $\alpha>1$.

In order to study in more detail the effect of the width of the openings, three models corresponding to a=b=20 meters, H=60, 90 and 120 meters (H/a=3, 4.5 and 6 respectively) were studied. The distance between two openings of these models is set equal to 3 meters. The sizes of the openings are shown in Fig. 7 while the results obtained are shown in Fig. 8. It is found that shear lag effect in core walls with openings are much severer than that in core walls without openings, even when the width of the openings is small. However, once openings are present, the width of the openings only has minor influence and the effect is the smallest when H/a=3.0. With a bigger value of H/a, the effect of the width of the openings becomes more significant. Moreover, it should be pointed out for all core walls with small H/a ratio, $\alpha>1$ for the entire height of the core wall which indicates that stress with opposite sign to the flange-web junctions develops at the center of the flange.

## 2.3 Effects of stiffening levels

In addition to the effect of different geometrical parameters, core walls with stiffening levels had also been studied. Three core walls with stiffening level and a=b=20 meters consisting 20, 30 and 40 levels respectively were analyzed (Fig. 9). For the 20-storey core wall, the stiffening level is located at the $11^{th}$ level while the stiffening levels are located at the $11^{th}$ and $21^{st}$ levels and the $11^{th}$, $21^{st}$ and $31^{st}$ levels for the 30-storey and 40-storey core walls

respectively. Figs. 10a to 10c show the shear lag coefficients obtained for these three core walls respectively. It can be seen that when stiffening levels are introduced, shear lag effect are affected. However, if the ratio H/a is small, the change has only minor influence on the value of $\alpha$. With the increase of the ratio H/a, the effect becomes relatively large. Moreover, the influence occurs along the whole height of the core walls and not only limited to the storeys adjacent to the stiffening levels.

## 3 Shear lag in multi-cell box girders

The reasons causing shear lag phenomena for single cell box girders and multi-cell box girders are somehow different. For single cell box girders under vertical loading that is symmetrical about the longitudinal axis of the girder, equal shear flows are transmitted from the webs to the edges of the flange. The resulting shear lag effect leads to a symmetrical distribution of the longitudinal stress in the flange. In contrast, as shown in Fig. 11, the shear flow from an internal web (point C) of a multi-cell girder is transmitted to *two* adjacent flange plates, whereas the shear flow from an external web (point A), is transmitted to only one adjacent flange. Thus, shear lag analysis of a multi-cellular girders is more complex than that for a single-cell girder.

The adaptive finite element analysis procedure used in the analysis of single cell box girders can be easily extended to tackle shear lag problems of multi-cell box girders. Fig. 12 shows the adaptive meshes used in the study of a simply supported three-cell box girder. From Fig. 12, it can be seen that refinement was again mainly carried out near the supports of the girder due to the sharp stress gradient there [6].

A number of parametric studies were conducted to analyze the shear lag effect of multi-cellular box girders. The effective breadth ratio, $\psi$, is again used to measure the shear lag effects. For multi-cell box girders, it is found that the shear lag effect is mainly depended on

(i) the loading type,

(ii) the ratio of the span length to the flange width (L/A) and,

(iii) the ratio of the flange width to the web height (a/b) (Fig. 13).

Both inclining webs and unequal cellular widths may affect the shear lag effect and therefore numerical studies were also conducted to investigate their effects.

### 3.1 Effects of the ratios a/b and L/A

A simply supported three-cell box girder as shown in Fig. 13 with a=c=A/3 was taken as the first example. Both the central point loading and uniformly distributed loading were considered. The effective breath ratio obtained are shown in Figs. 14 and 15 respectively. Fig. 14 indicates that when under the action of central point loading, the value of a/b severely affects the value of $\psi$. However, with the increase of the ratio L/A, the effect become smaller and smaller. Normally, for a given value of L/A, the value of $\psi$ increases as a/b decreases. The ratio L/A is a crucial factor that affects the shear lag and the larger the value of L/A, the bigger the value of $\psi$, which implies a smaller shear lag effect. The variation of $\psi$ mainly takes place near the supports and the loading point where the value of $\psi$ is close to zero. The reduction of $\psi$ also depends on the ratio a/b. In general, the smaller the value of a/b, the larger the reduction in the loading point position. The change of the ratio a/b does not cause much variation of $\psi$ near the supports.

Fig. 15 indicates that under the action of uniform distributed loading the variation of $\psi$ mainly occurs near the supports, which is different from the case of central point loading. The effects of the ratios a/b and L/A are similar to the point load case. The ratio a/b affects seriously the value of $\psi$ when the value of L/A is small and a smaller value of a/b leads to a bigger shear lag effect near the midspan. Again, the ratio L/A is the key factor and increasing the value of L/A results in an increase of $\psi$ except for the sections adjacent to the supports.

### 3.2 Effects of the inclined web plates

Box girders with inclined web plates are not exceptional and are widely used in bridge engineering. Web plates with inclined angles will obviously affect the shear lag of the top flanges. Six different simply supported three-cell box girders were analyzed and their cross-sections are shown in Fig. 16. The span length and the top flange width ratios (L/A) for them are all equal to 5/3. Both central point loading and uniformly distributed loading were considered. Fig. 17 illustrates the effects of the inclined webs. In general, the effect of inclined webs may be neglected under the action of point load except near the supports. However, when the girders are under uniform loading, the inclined webs cause significant variations of $\psi$. Particularly, if one only considers the shear lag effect, a three-cell box girder with vertical webs is the worst and the webs with an appropriate inclining angle can efficiently decrease the shear lag effect. However, the optimal angle cannot be found in advance and can only be obtained by numerical experiments. For the three-cell box girder shown in Fig. 16, the optimal angle is approximately equal to 37.5°.

### 3.3 Effects of unequal cellular widths on three-cell box girder

In engineering applications, the cellular widths of a box girder may be adjusted according to practical needs. The change of cellular widths will inevitably affect the shear lag of the section. Fig. 13 shows a three-cell box girder whose central cell width is different from the first and third cells. For convenience, the dimensions of the girder were made to satisfy the following conditions during the numerical studies:

(i) the overall width (A) of the top flange was kept constant,

(ii) different cellular width ratios were achieved by changing the width of the central cell, c, from 0 to A.

It should be noted the value of c will affect the type of the box girder. When c=0, the girder is reduced to a double-cell box girder. While if c=A, the girder becomes a single-cell box girder. For 0<c<A, the girder is a three-cell box girder. The box girder is simply supported with aspect ratio L/A equal to 10/3. Both the cases of central point load and uniform loading were studied.

The variations of effective breadth ratio for different geometries are shown in Fig. 18. Fig. 18 indicates that variation of the cellular widths severely affects the shear lag effect and when c=A, the shear lag effect is the largest. The relationship between c/A and the value of $\psi$ is plotted in Fig. 19 to further study its effect on $\psi$. Fig. 19 illustrates that the value of $\psi$ is the smallest when c=A. Furthermore, if 0<c<A and the girder is a three-cell box girder, the situations are not always better than the case of c=0. An optimum value of c might exist that could result in the smallest shear lag effect. However, it is difficult to find out a single optimum value of c for both cases and for all the sections along the span. From Fig. 19, it can be seen that a value of c between 0.1A to 0.3A may considerably reduce the shear lag effect of the girder.

## 4 Shear lag analysis of curved box girder

The use of horizontal curved girders has increased considerably in recent years since it can provide a more aesthetically pleasing structure with its streamlined appearance. However, curved girders are subjected to both flexural stresses and significant amounts of torsional stresses (torsional shear stress and warping normal stress) which will complicate the shear lag effect. In curved box girder, shear lag phenomenon will refer to the non-uniform distributions of the normal stress in the x' direction (Fig. 20). Fig. 21 shows the typical normal stress distribution across the top flange of a curved box girder where positive shear lag occurs. Due to the present of torsional stress, the normal stress distribution across the flange is

unsymmetrical and the stresses at the two junctions are different. The same adaptive procedure based on the thick shell model is again used for the study of the shear lag problem for this type of structure.

Fig. 22 shows the adaptive meshes generated during the study of a simply supported curved box girder. It can be seen that refinement again mainly occurs near the supports. Since the stress near the supports is small comparing to that of other parts of the model, it is not necessary to use a highly refined mesh [6] and as a result a value of $e_a$ =5% was again used all the numerical studies. In order to cover a wide range of practical situations, a number of parametric studies had been conducted. Besides loading types and support conditions, the shear lag of curved box girders may be affected by other geometrical parameters including the radius of curvature/flange width ratio (R/b) and the web width/flange width ratio (a/b).

### 4.1 Simply supported curved box girders

Firstly, a single-span, simply supported curved box girder with $2\theta=90°$, where $\theta$ is the half-central angle, was studied (Fig. 23). Totally 30 models were analyzed. The radius of curvature/flange width ratios (R/b) of the models were varied from 10 to 20 (in steps of 10, 15 and 20), while the web width/flange width ratios (a/b) were varied from 1/3 to 3 (in steps of 1/3, 1/2, 1, 2 and 3). The loading conditions are shown in Fig. 24.

In Figs. 25 and 26, the effective breath ratio, $\psi$, of the simple supported curved box girder are plotted against $\vartheta$ for the central point load and uniformly distributed loading cases respectively. Basically, the shapes of all $\psi$ curves of for different situations are similar. The value of $\psi$ is small near the support and increases rapidly to a peak value. After the peak value, $\psi$ falls and levels off at some position until the midspan. The value of $\psi$ near the midspan is much larger than that near the support. From Figs. 25 and 26, it can be seen that loading type *does not* significantly affect the shear lag of a curved box girder under simply

supported condition when R<20. Figs. 25 and 26 also indicate that the ratio a/b may affect the shear lag severely and the peak values and positions of ψ are changed when a/b changes. With the increase of a/b, the location of the peak point moves gradually towards the midspan. The effects of R/b on ψ when a=b for different ratios of R/b are shown in Fig. 27. It can be seen that the effect of the ratio R/b on ψ mainly takes place at where the slope of ψ is steep and is relatively insignificant in the other parts of the girder.

### 4.2 Curved box girders with different radii of curvature

In order to study the effect of the radius of curvature, R, on the shear lag effect, curved box girders with different radii of curvature were analyzed. As shown in Fig. 28, the two end points of the girder (A and B), were fixed and the distance between them is equal to 28.28 meters. Six different box girders were generated to link the two points. The radius of curvature to the flange width radios (R/b) of them are in turn equal to 162.26, 81.44, 54.64, 28.3, 20 and 16.33 which are corresponding to half-central-angles (θ) of 5°, 10°, 15°, 30°, 45° and 60° respectively. All the girders are simply supported and both central point load and uniformly distributed loading cases were considered.

The results obtained are plotted in Fig. 29 for different ratios of a/b. From the results obtained in the last section, it is known that different loading types only slightly affect the effects of different geometrical parameters on shear lag for a simply supported, one-span curved box girder. Therefore, only the results for the point load case are shown in Fig. 29. (The effects of different geometrical parameters obtained from the uniformly distributed loading case are very similar to the case of point loading and hence omitted here.) Fig. 29 shows that the radius of curvature of the girder affects the effects of a/b on the value of ψ. With the decrease of R/b, the effect of a/b on ψ becomes severer and severer. For a given value of R/b, increasing the

value of a/b moves the peak point of the $\psi$ curve towards the midspan. However, when the value of a/b is less than 1, both the ratios a/b and R/b do not have much effect on $\psi$.

In order to find out more details for the effect of the radius of curvature (and hence, $\theta$, the half-central angle of the girder) on $\psi$, the variation of $\psi$ corresponding to different values of $\theta$ are plotted in Fig. 30. Again, only the results for point load case are shown. It can be seen that the variation of $\theta$ has obvious influence on shear lag. Moreover, the effect becomes more and more significant when the ratio a/b is increased. For a given value of a/b, the peak point of the curve of $\psi$ gradually moves to the midspan with the increase of $\theta$ (decrease of radius of curvature). When the ratio a/b is less than 1, the curves of $\psi$ with different radii of curvature are approximately parallel to each others from the peak point to the midspan. In general, the smaller the central angle, the bigger the value of $\psi$ and hence the smaller the shear lag effect. It is known [6] that aspect ratio is an important factor affecting shear lag of straight box girders and the larger the aspect ratio the smaller the shear lag effect. However, it should be noted that the situation for curved box girder is different. Since the aspect ratio of a curved box girder is equal to $c\theta/(b\sin\theta)$, where c is half the distance between the two supports (Fig. 28), the aspect ratio of a curved box girder will increases as $\theta$ (hence $\theta/\sin\theta$) increases. From Fig. 30, it can be seen that when $\theta$ increases, $\psi$ reduces and the shear lag effect becomes more serious. Therefore, it can be concluded that the effect of aspect ratio on shear lag in curved box girders is *opposite* to that in straight box girders.

### 4.3 Negative shear lag in curved box girder

In Part 1 of this study, the negative shear lag problems for straight cantilevered box girders has been analyzed by the adaptive refinement procedure. For curved box girders, negative shear lag can also take place for the case shown in Fig. 31 where brackets are present on the two sides of the girder.

Fig. 32 shows the typical normal stress distribution across the top flange for the simply supported girder shown in Fig. 31 with c/b=1 and a/b=1 under the action of a central point load. It can be seen that the maximum normal stress does not occur at any one of the two flange-web junctions and negative shear lag [11-13] takes place. In here, a dimensionless parameter $\varepsilon$ defined as

$$\varepsilon = \frac{\sigma_{max}}{Max(\sigma_A, \sigma_B)} \tag{1}$$

will be used to distinguish the type of shear lag occurs in the section. In Eqn. 1, $\sigma_{max}$ is the maximum normal stress in the cross section while $\sigma_A$ and $\sigma_B$ are the normal stresses at the two flange-web junctions respectively. If $\varepsilon$ is equal to 1, positive shear lag occurs while $\varepsilon > 1$ implies that negative shear lag takes place. Since in general, the location of the maximum normal stress is not known in advance, $\varepsilon$ cannot reflect the distribution of normal stress across the flange. Thus, the effective breadth ratio $\psi$ will again be used to indicate the degree of shear lag of the structure.

### 4.3.1 Parametric studies

The geometrical parameters studied here include the breadth of bracket/web plate spacing ratio (c/b), the web width/web plate spacing ratio (a/b) and the radius of curvature/web plate spacing ratio (R/b). Totally 60 models were analyzed. The values of c/b used were in turn set equal to 0.1, 0.3, 0.5 and 0.8. The ratios a/b and R/b are varied from 1/3 to 3 (in steps of 1/3, 1/2, 1, 2 and 3) and from 10 to 20 (in steps of 10, 15 and 20) respectively. All the models studied are simply supported and both the actions of central point load and uniformly distributed loading were considered.

As it has been shown in Section 4.1, the loading type does not seriously affect the effects of different geometrical parameters for a simply supported, one-span curved box girders.

Therefore, only the results obtained under central point load are presented to illustrate the effect of the geometrical parameters.

Figs. 33 to 35 show the effect of the ratio c/b on the shear lag. It can be seen that when the bracket width, c, is larger than 0, negative shear lag ($\varepsilon>1$) occurs along the whole span of the curved box girder for all the values of R/b and a/b. This further indicates that negative shear lag is quite common for curved box girders. In general, the largest value of $\varepsilon$ occurs near the supports and $\varepsilon$ decreases gradually to the midspan, which means that severer negative shear lag takes place near the supports. The degree of negative shear lag is seriously affected by the ratio c/b, except for a small part of the girder near the support. In addition, no matter what are the values of R/b and a/b, increasing the value of c/b results in an increase $\varepsilon$ which indicates severer negative shear lag effect takes place. Hence, it may be said that the ratio c/b is a significant factor affecting negative shear lag. Effective breadth ratio is also calculated to reflect the degree of non-uniform distribution of normal stress. It can be seen from Figs. 33f to 35f that the shapes of the curves when $c>0$ (girder with brackets) are similar to that when $c=0$ (girder without bracket). However, when $c>0$, the value of $\psi$ is smaller than that obtained from $c=0$ and the change of the ratio c/b only slightly affects the values of $\psi$ between the support and the peak point of the curve, but largely influences the value of $\psi$ from the peak point to the midspan. Figs. 33 to 35 also show that both the ratios R/b and a/b only have minor effect on negative shear lag and increasing the values of them will move the peak point of the curve of $\psi$ closer to the midspan.

## 5 Conclusions

In this study, parametric studies of shear lag for complex plated structures including core wall with openings, multi-cell box girder and curved box girder have been carried out by the

adaptive finite element analysis procedure. The following conclusions can be drawn from the numerical results:

(1) For core wall with openings, the shear lag coefficient $\alpha$ is mainly dependent on the height to web ratio (H/a). The degree of shear lag varies along the height and generally increases from the fixed end to the free end. Openings in a core wall severely increase the shear lag effect and the bigger the size of the openings, the severer the shear lag effect.

(2) For multi-cell box girder, the length to width ratio (L/A) is the most important factor affecting shear lag. The cell width to cell height ratio (a/b) also mildly affects the shear lag effect. Furthermore, an appropriate inclined web angle might minimize shear lag effect. The change of the cellular widths of a three-cell box girder also affects the shear lag effect and an optimum case exists in which the shear lag effect is reduced to a minimum.

(3) For curved box girder, geometrical parameters such as the web width/flange width ratio (a/b) and the radius of curvature/flange width ratio (R/b) can significantly affect the shear lag effect. For a simply supported, one-span curved box girder, the effect of loading type is not the most significant factor. The effect of aspect ratio on shear lag in curved box girder is reversed to that of straight box girders. Negative shear lag may also occur in curved box girders with brackets and it is found that the bracket width/web plate spacing ratio is the most important factor affecting negative shear lag.

**References**


1. V. Kristek, J. Studnicka and M. Skaloud, Shear lag in wide flanges of steel bridges, *ACTA Tech. CSAV* **26**, 464-488 (1981).

2. V. Kristek, Folded plate approach to analysis of shear wall systems and frame structures, *Proc., Instn. Civ. Engnrs*., **67**, 1065-1075 (1979).

3. H. R. Evans, and A. R. Taherian, A design aid for shear lag calculations, *Proc., Instn. Civ. Engrg*., **69**, 403-424 (1980).

4. N. Tahan and M. N. Pavlovic, Shear lag revisited: the use of single Fourier series for determining the effective breadth in plated structures, *Compt. Struct*. **63**, 759-767 (1997)

5. A. K. H. Kwan, Simple method for approximate analysis of framed tube structures, *J. Struct. Engrg*., ASCE, **120**, 1221-1239 (1994)

6. C. K. Lee, and G. J. Wu, Shear lag analysis by adaptive finite element method: Part 1: Shear lag in simple plated structures. To appear in *Thin-walled Structures*.

7. O. C. Zienkiewicz and R. L. Taylor, The finite element method, Vol. 2 Solid and fluid mechanics, Dynamics and non-linearity, Fourth Edition, McGraw-Hill Book. Co. 1991.

8. LUSAS, MYSTRO User Guide, FEA, Ltd, UK, 1997

9. LUSAS, LUSAS User Guide, FEA, Ltd, UK, 1997.

10. LUSAS, MYSTRO Command Reference I and II, FEA, Ltd, UK, 1997

11. S. T. Chang, and F. Z. Zheng, Negative shear lag in cantilever box girder with constant depth, *J. Struct. Eng*., ASCE, **113**, 20-35 (1987)

12. V. Kristek, and J. Studnicka, Discussion of "Negative shear lag in cantilever box girder with constant depth" by Chang S. T. and Zheng F. Z. *J. Struct. Eng*., ASCE, **114**, 2168-2173 (1988)

13. H. Nakai and Y. Murayama, Researches on negative shear lag of cantilever beams and application to bridge design, *Trans. JSCE* **8**, 107-109 (1976)

Pre-printed version for the paper appeared in the journal
Thin-Walled Structures, Vol. 38, 2000, 311-336

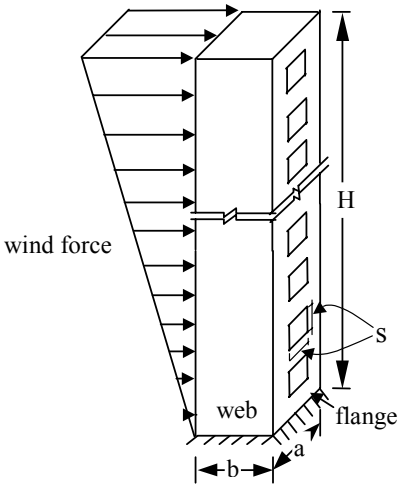


Fig. 1 A core wall with openings

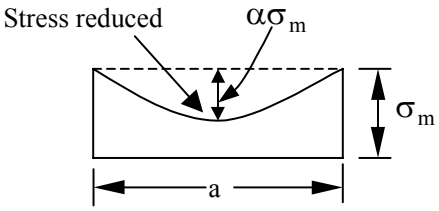


Fig. 3 Longitudinal stress distribution in flange and definition of α

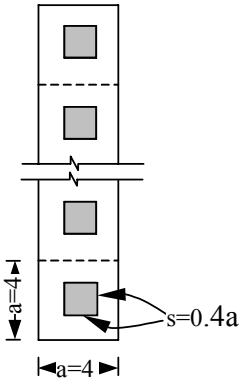


Fig. 4 Openings of a core wall

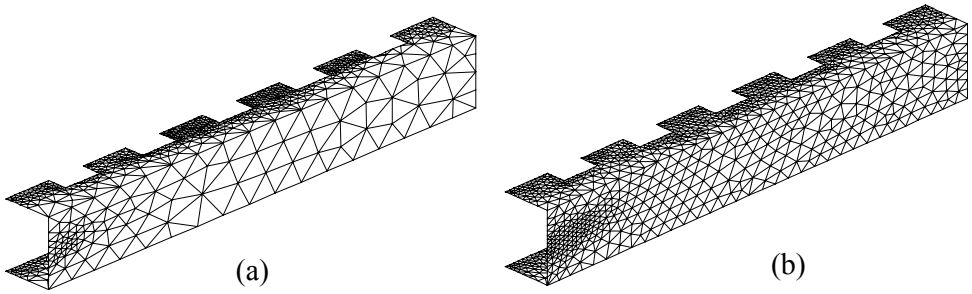


Fig. 2 Meshes generated during adaptive analysis: (a) initial mesh (b) final mesh

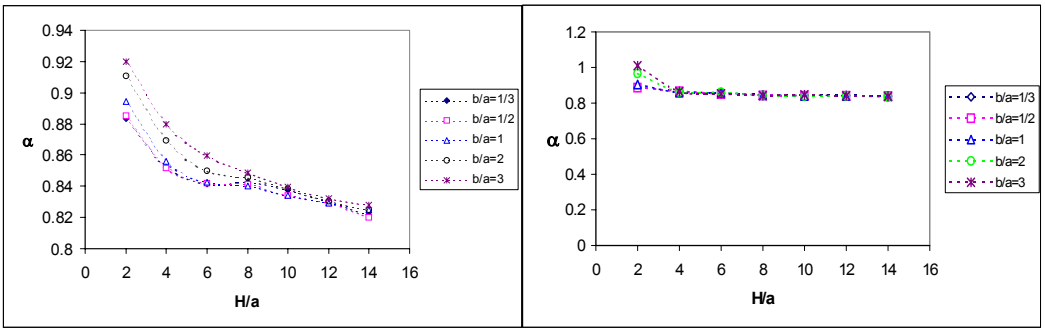


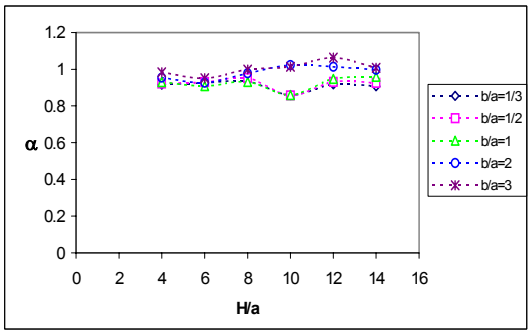


Fig. 5 Values of α at: (a) the fixed end (b) the middle (c) the top wall

Pre-printed version for the paper appeared in the journal
Thin-Walled Structures, Vol. 38, 2000, 311-336

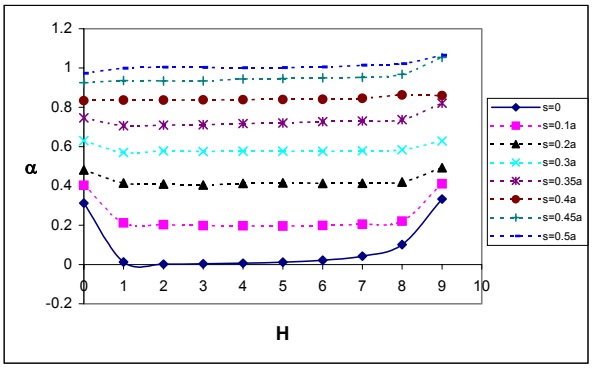


Fig. 6 Values of α at each floor of the core wall with openings of different sizes

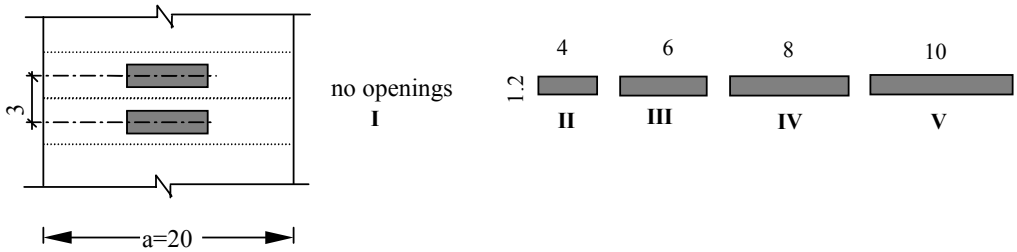


Fig. 7 The dimensions of the openings

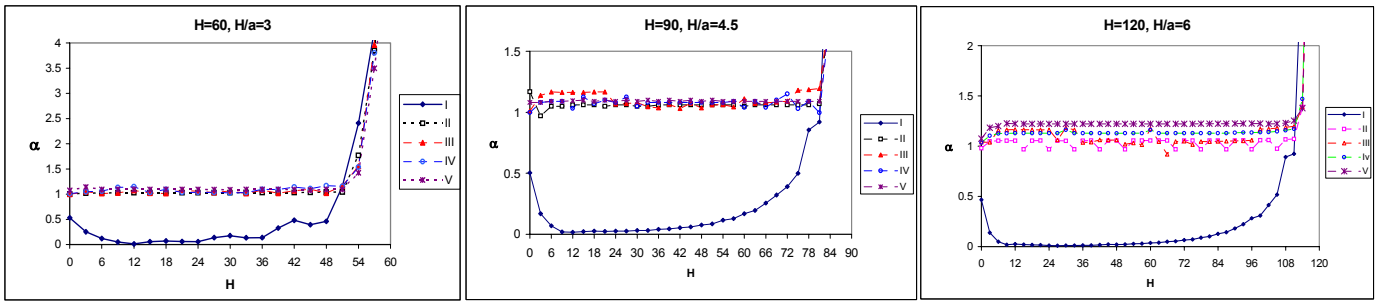


(a) (b) (c)

Fig. 8 Values of α for three models with different opening widths
(a) H/a=3 (b) H/a=4.5 (c) H/a=6

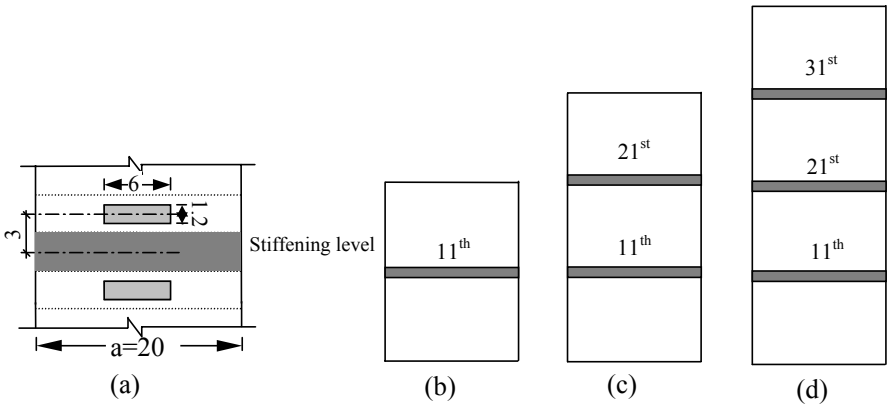


(a) (b) (c) (d)

Fig. 9 The core walls with stiffening levels
(a) the dimension of the openings and stiffening level (b) H/a=3 (c) H/a=4.5 (d) H/a=6

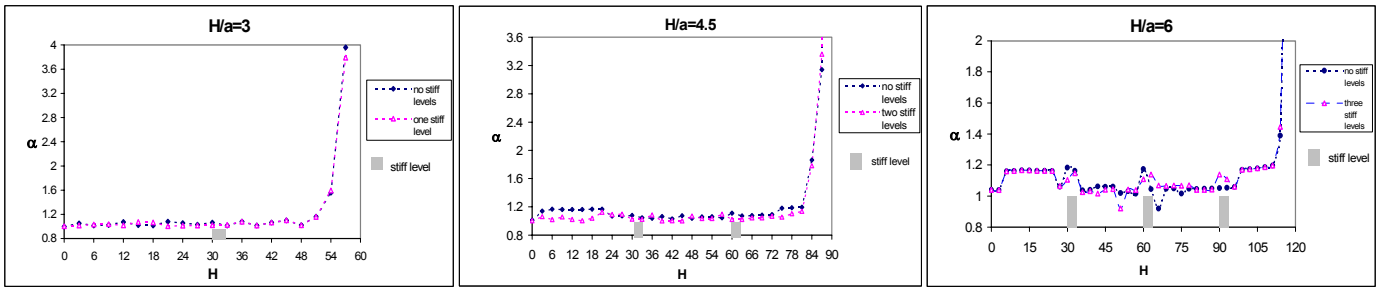


(a) (b) (c)

Fig. 10 Results of core walls with stiffening levels
(a) α for H/a=3 (b) α for H/a=4.5 (c) α for H/a=6

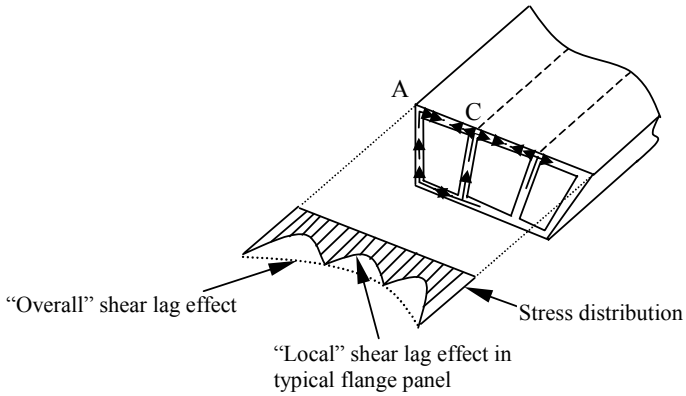


Fig. 11 Longitudinal flange stresses in multi-cell box girders

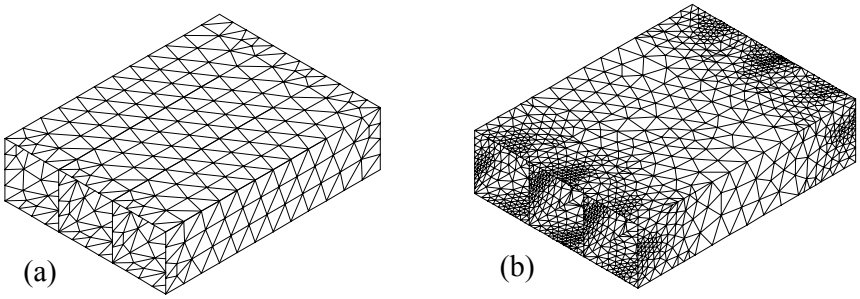


Fig. 12 Meshes generated during adaptive analysis: (a) initial mesh (b) final mesh

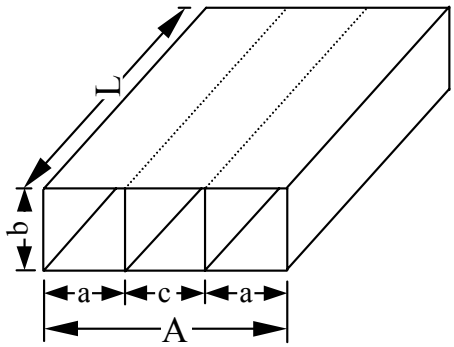


Fig. 13 A three-cell box girder

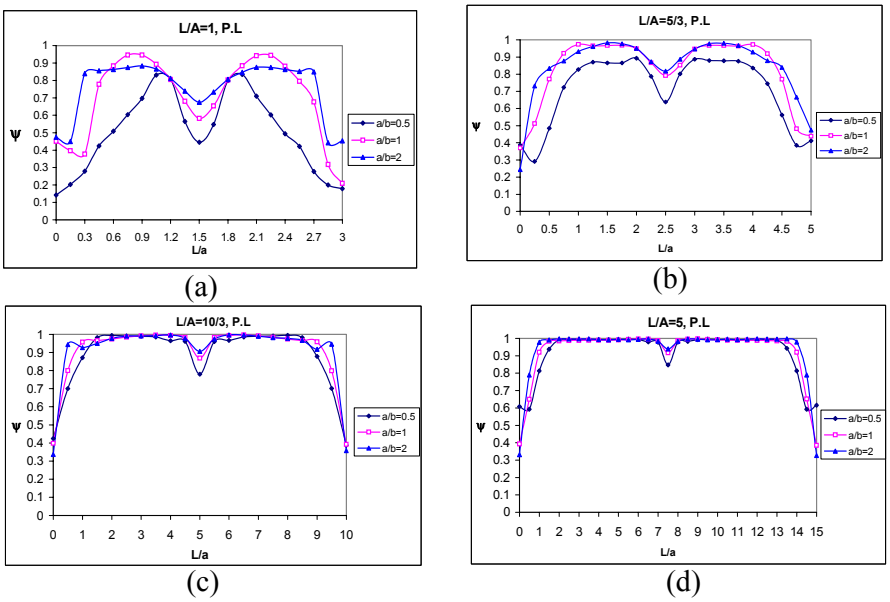


Fig. 14 Effective breadth ratio along the span (point loading)
(a) L/A= 1 (b) L/A= 5/3 (c) L/A= 10/3 (d) L/A= 5

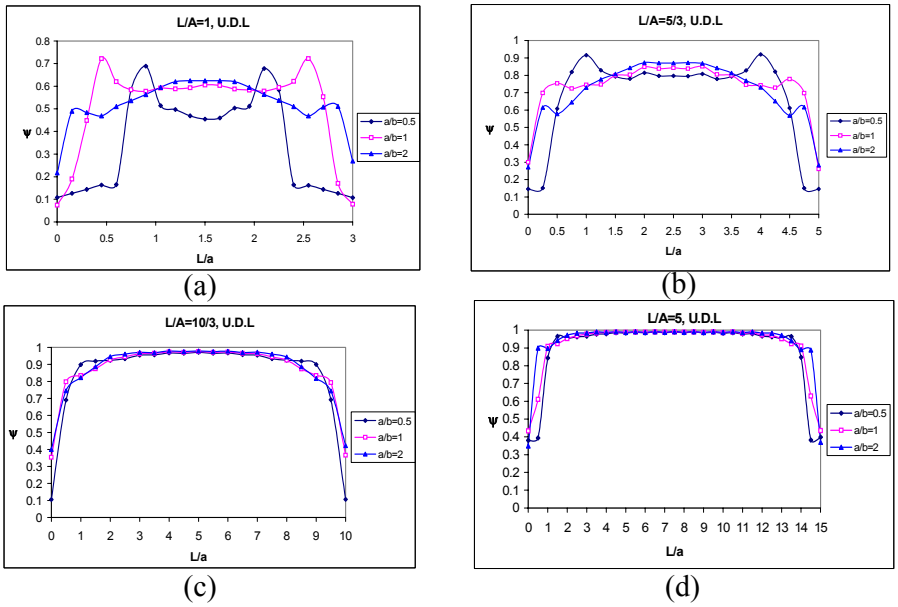


Fig. 15 Effective breadth ratio along the span (uniformly distributed loading)
(a) L/A= 1 (b) L/A= 5/3 (c) L/A= 10/3 (d) L/A= 5

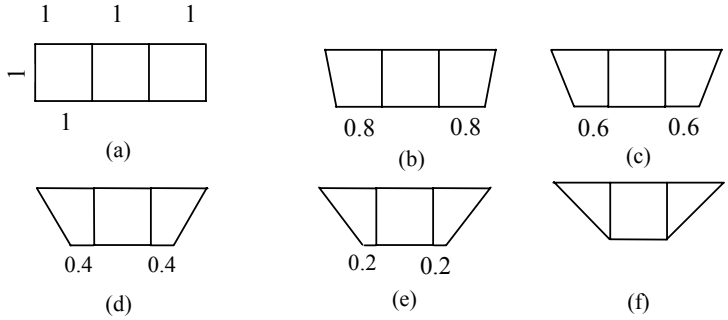


Fig. 16 Cross-section of different three-cell box girders

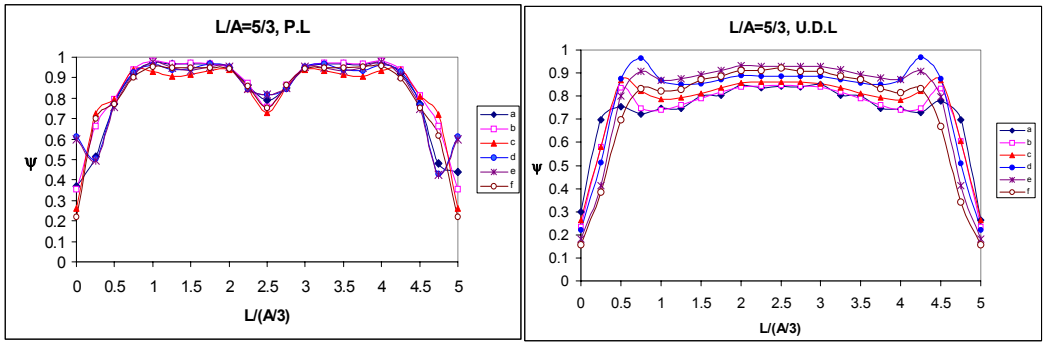


(a) (b)

Fig. 17 Effects of the inclined webs on the value of ψ
(a) point loading (b) uniformly distributed loading

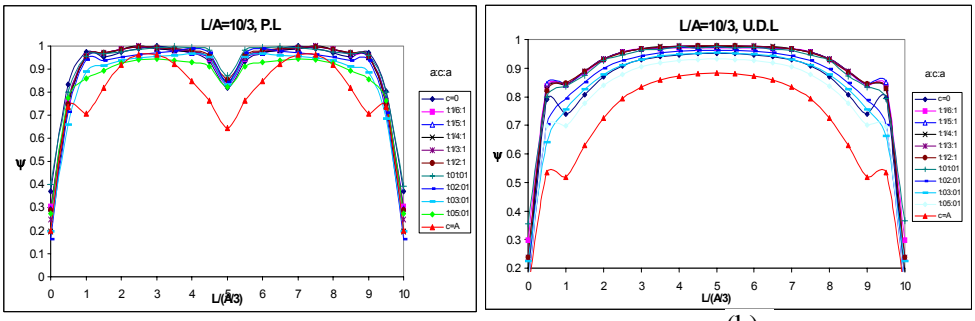


(a) (b)

Fig. 18 Results of ψ for three-cell box girders with different cellular widths
(a) point load (b) uniformly distributed loading

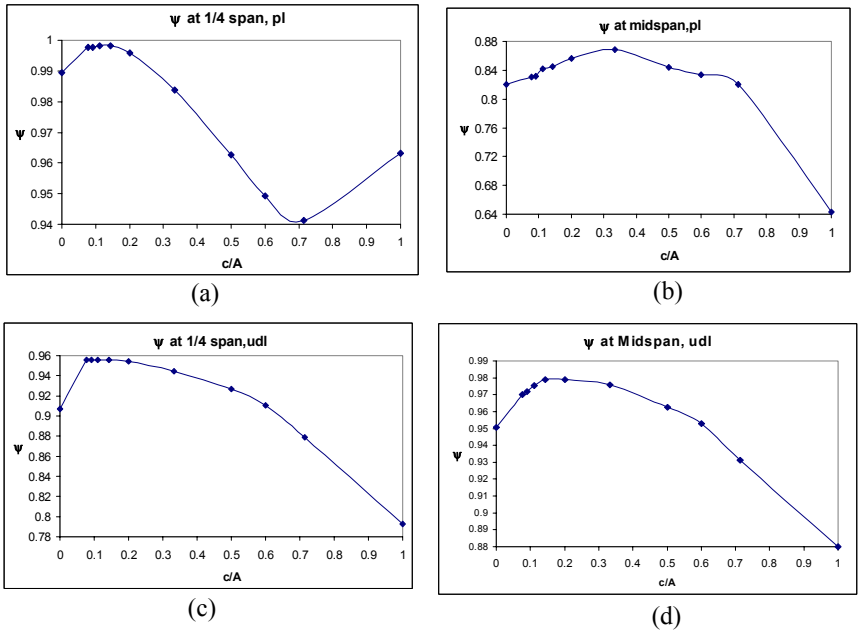


(a) (b)

(c) (d)

Fig. 19 Results of ψ of a three-cell box girder (a) Point loading at midspan (b) point loading at ¼ span (c) uniformly distributing loading at midspan (d) uniformly distributing loading at ¼ span

Pre-printed version for the paper appeared in the journal
Thin-Walled Structures, Vol. 38, 2000, 311-336

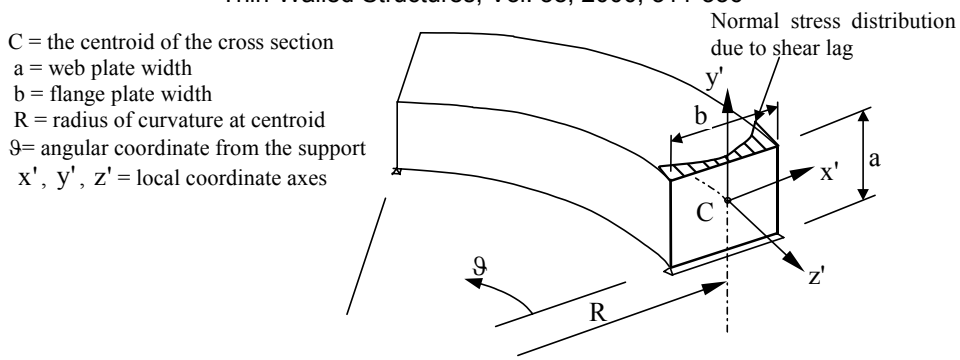


Fig. 20 A curved box-girder

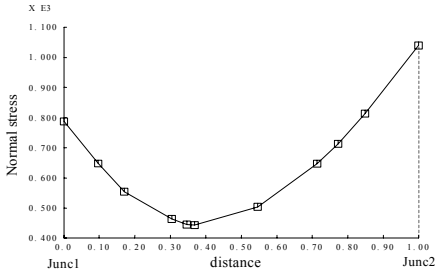


Fig. 21 Normal stress distribution of a simply supported curved box girder

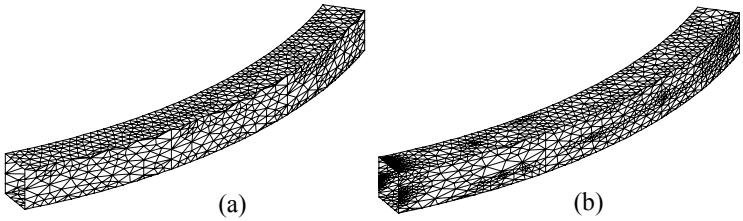


Fig. 22 Meshes generated during adaptive analysis: (a) initial mesh (b) final mesh

O: center of the girder
m: section under consideration
R: Radius of curvature
θ: half central angle
ϑ: angular coordinate of section
▬: Supports
X axis, Z axis: the global co-ordinate system in LUSAS

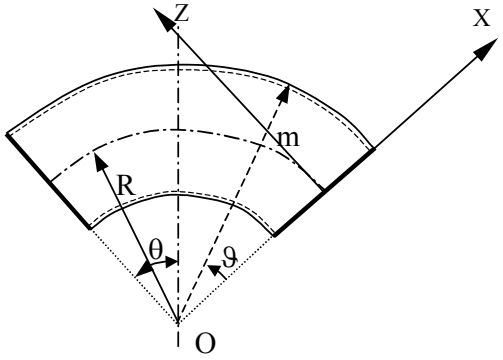


Fig. 23 Plan view of horizontal curved box girder

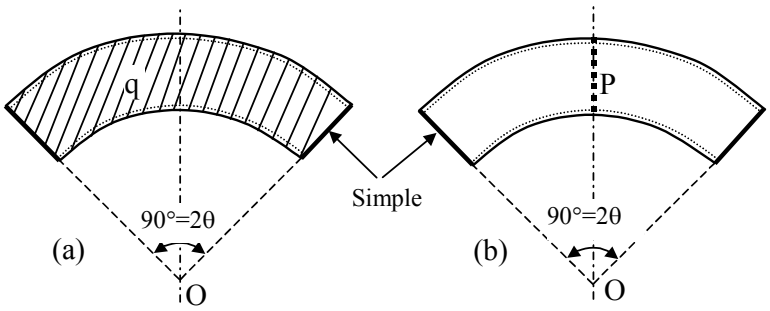


Fig. 24 Loading conditions: (a) uniformly distributed loading (b) central point load

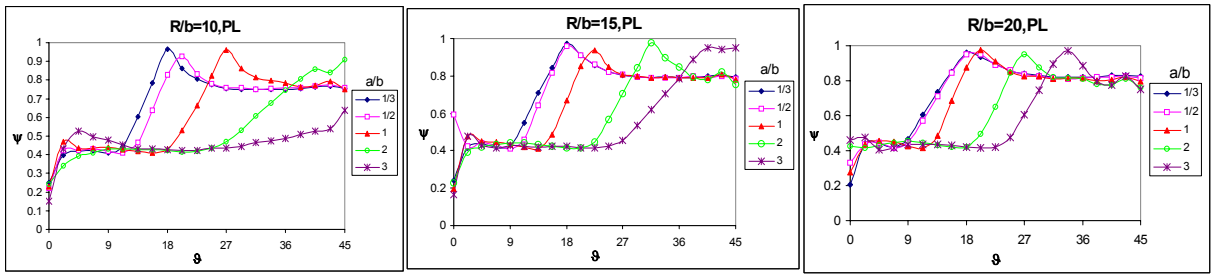


(a) (b) (c)

Fig. 25 Variation of ψ of single-span, simply supported curved box girders (point load) (a) R/b=10 (b) R/b=15 (c) R/b=20

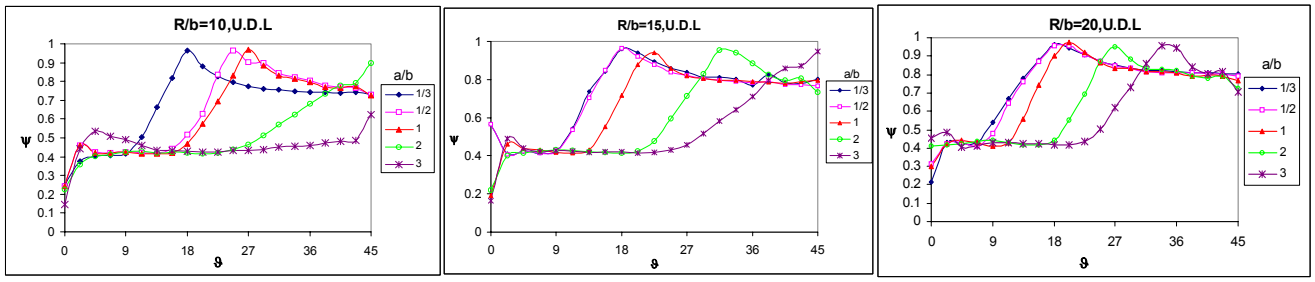


(a) (b) (c)

Fig. 26 Variation of ψ of single-span, simply supported curved box girders under uniformly distributed loading: (a) R/b=10 (b) R/b=15 (c) R/b=20

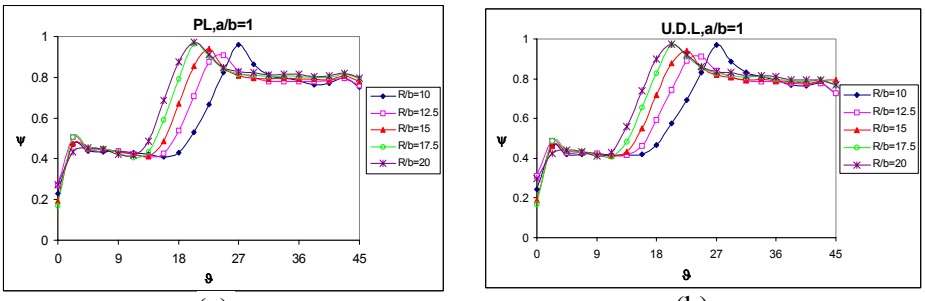


(a) (b)

Fig. 27 Variation of ψ of single-span, simply supported curved box girders for different R/b ratios: (a) point load (b) uniformly distributed loading

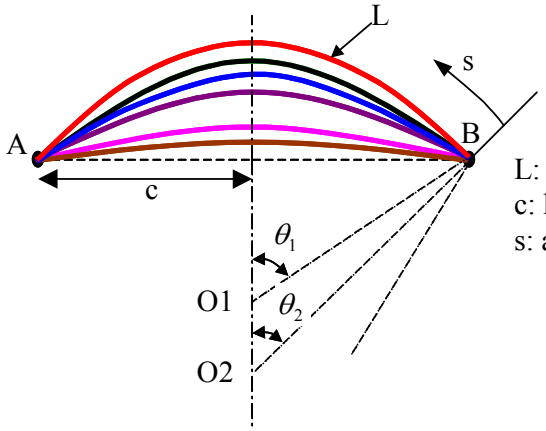


L: half arc length of the girder
c: half the distance between A and B
s: arc length meaured from the support B

Fig. 28 Curved box girders with different radii of curvature

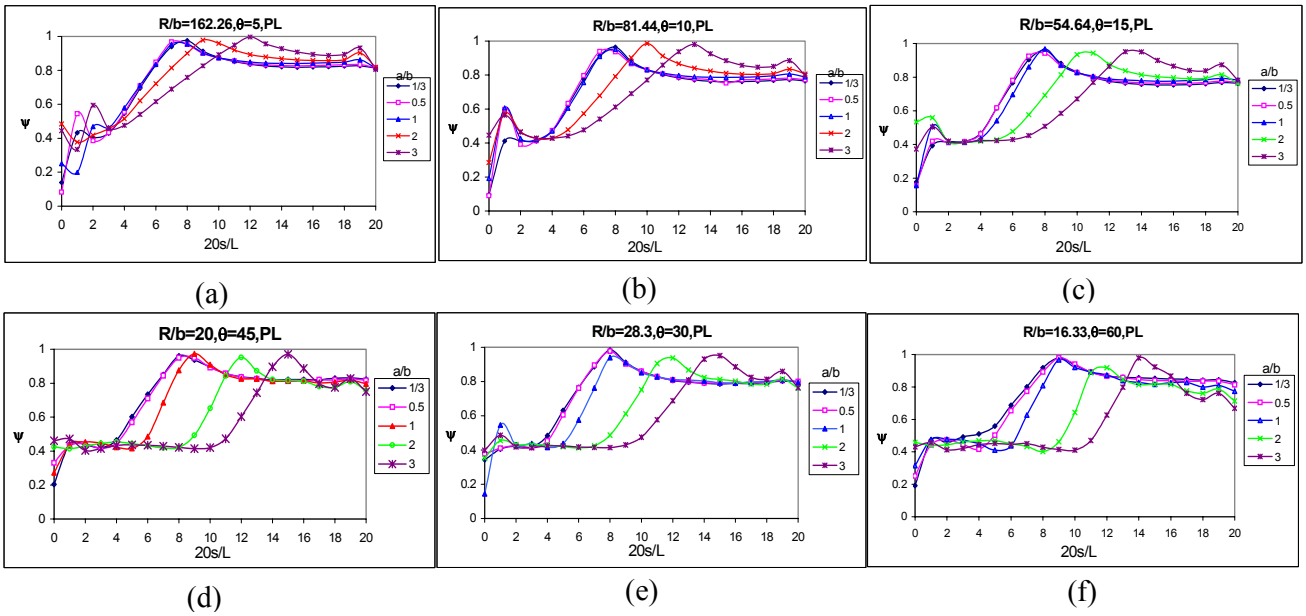


Fig. 29 The results of $\psi$ of six curved box girders with different radii of curvature (point load)

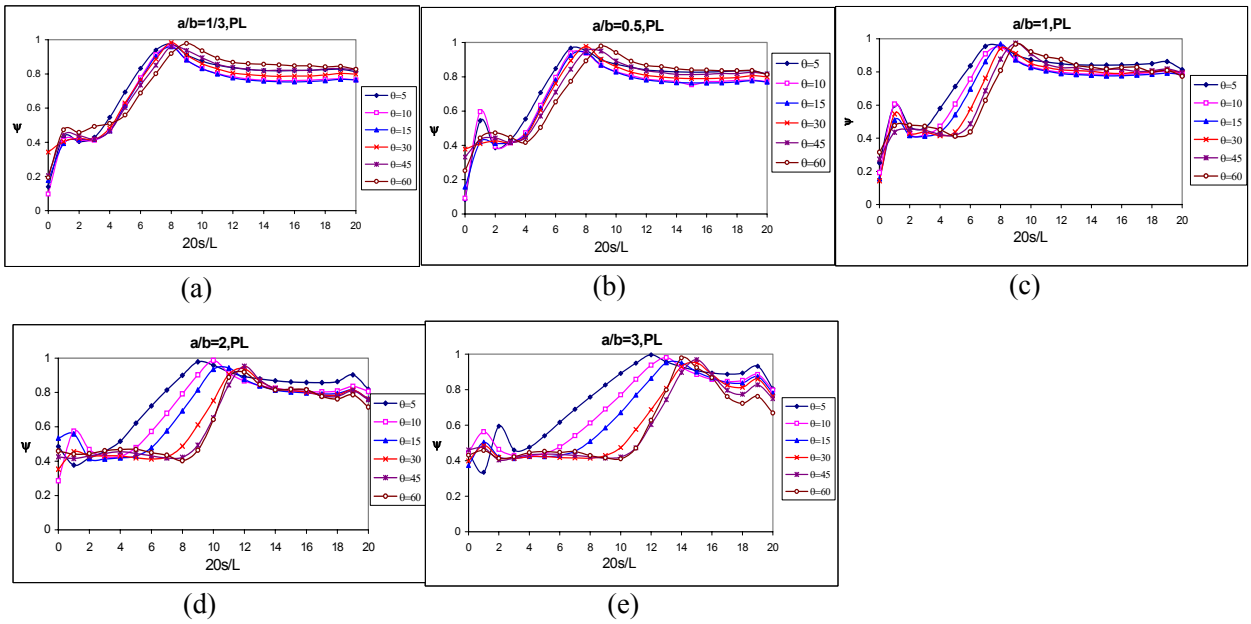


Fig. 30 The effect of radius of curvature on shear lag

C = Centroid of the cross section
a = web plate width
b = web plate spacing
c = breadth of bracket
R = radius of curvature at centroid
$\vartheta$= angular coordinate from the support
x', y', z' = local coordinate axes

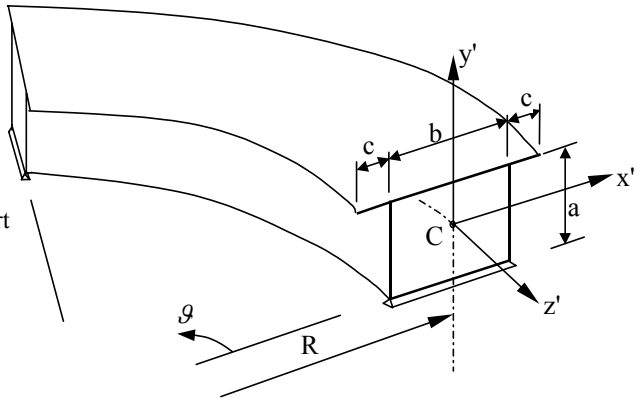


Fig. 31 Typical cross-section of a curved box girder for negative shear lag study

Pre-printed version for the paper appeared in the journal
Thin-Walled Structures, Vol. 38, 2000, 311-336

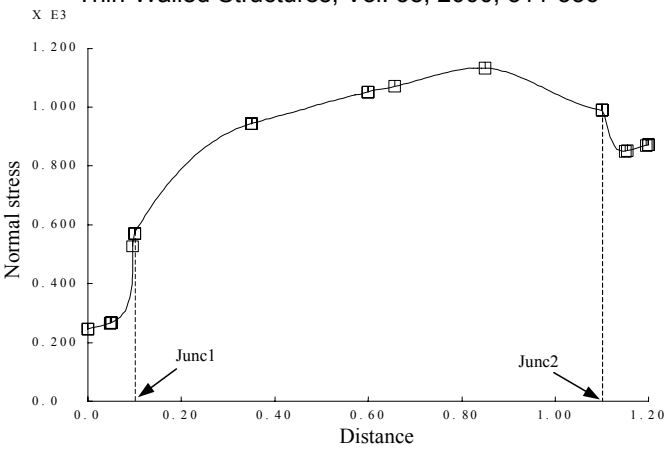


Fig. 32 Normal stress distribution across the top flange of a curved box girder

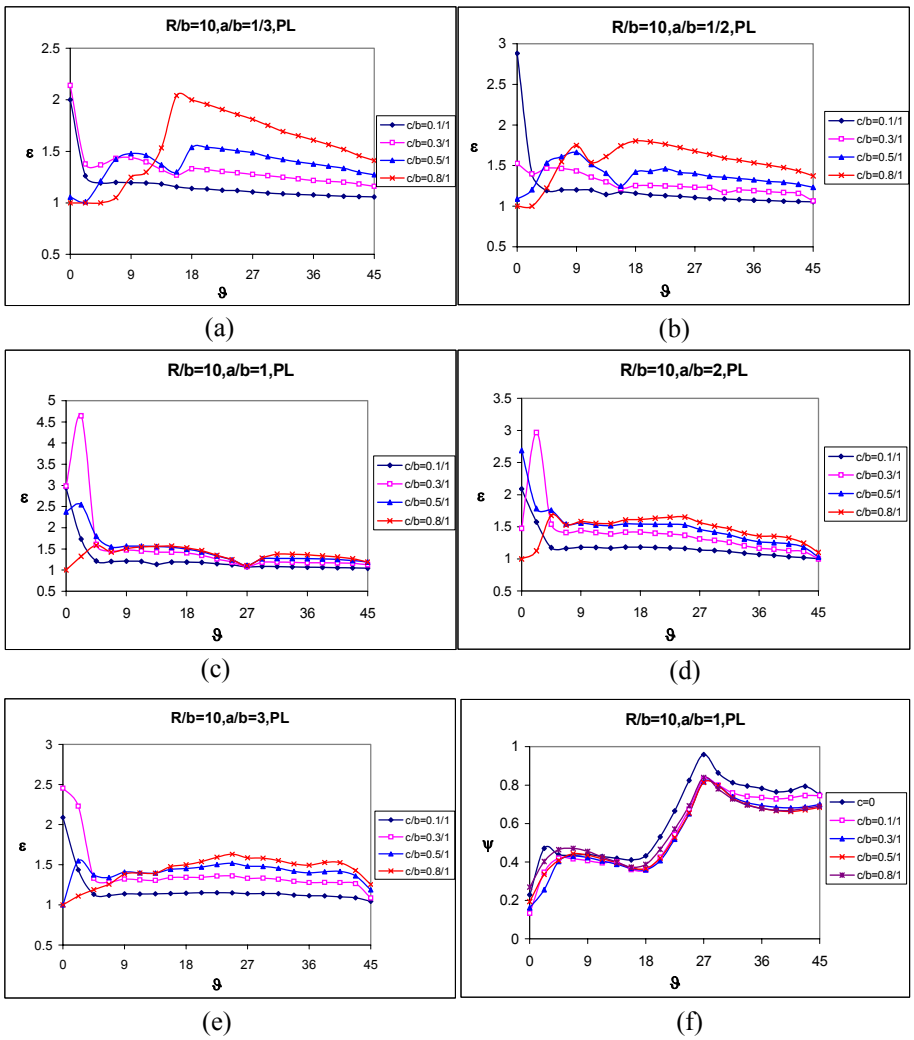


Fig. 33 Effect of c/b on shear lag (R/b=10, point load)
(a)~(e) the results of ε (f) the result of ψ

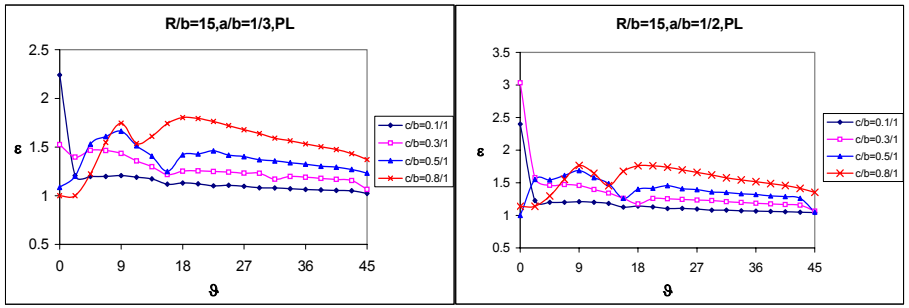


(a) (b)

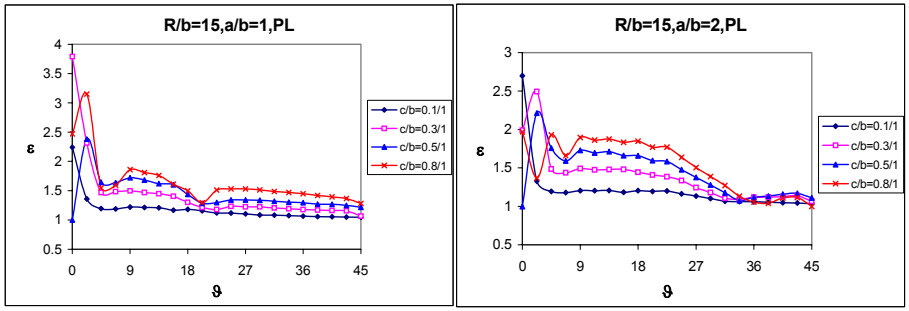


(c) (d)

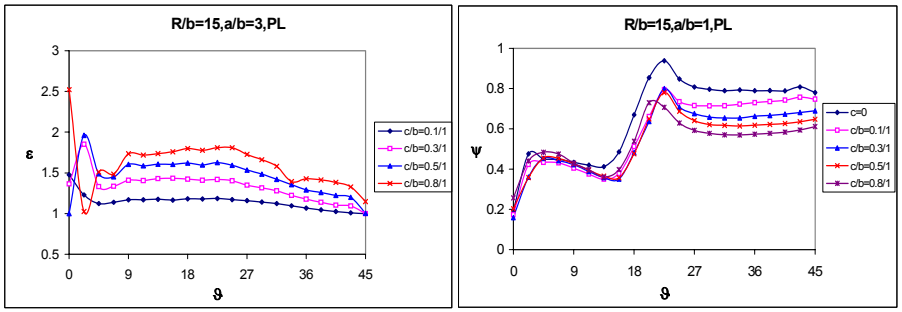


(e) (f)

Fig. 34 Effect of c/b on shear lag (R/b=15, point load)
(a)~(e) the results of ε (f) the result of ψ

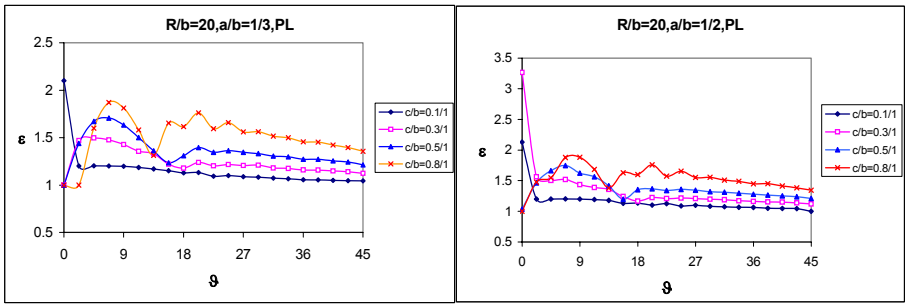


(a) (b)

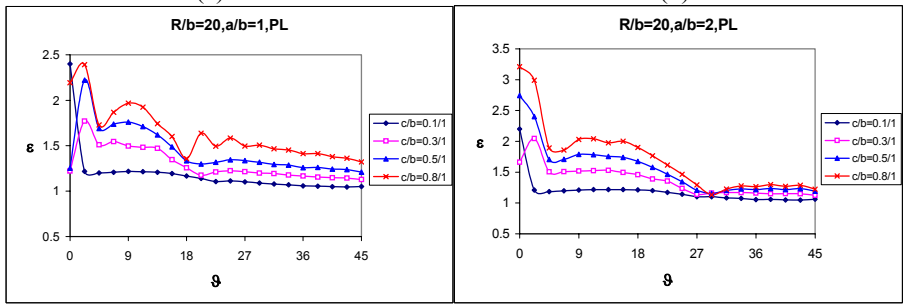


(c) (d)

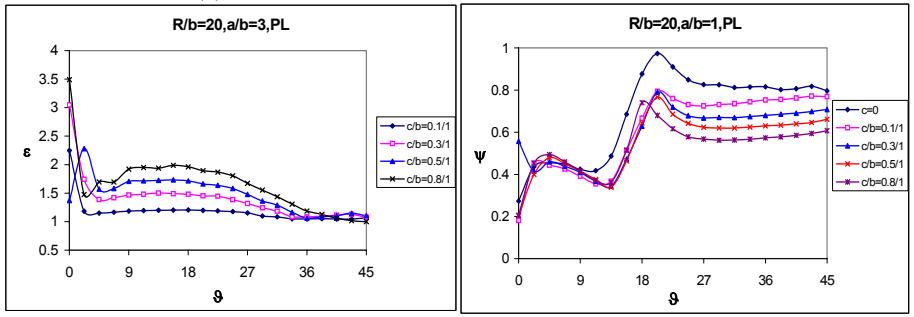


(e) (f)

Fig. 35 Effect of c/b on shear lag (R/b=20, point load)
(a)~(e) the results of ε (f) the result of ψ